Available online at www.sciencedirect.com
ScienceDirect
Food Research International 39 (2006) 1058–1066
FOOD RESEARCH INTERNATIONAL
www.elsevier.com/locate/foodres

The bubble size distribution in wheat flour dough

Guillermo G. Bellido [a], Martin G. Scanlon [a,*], John H. Page [b], Benedikt Hallgrimsson [c]

[a] Department of Food Science, University of Manitoba, Winnipeg, Manitoba, Canada R3T 2N2
[b] Department of Physics and Astronomy, University of Manitoba, Winnipeg, Manitoba, Canada R3T 2N2
[c] Department of Cell Biology and Anatomy, University of Calgary, Alberta, Canada

Received 26 June 2006; accepted 14 July 2006

Abstract

This paper reports, for the first time, the use of non-invasive microcomputed tomography (μCT) to unambiguously determine the bubble size distribution in doughs made from strong breadmaking flour. The doughs studied were comprised of two types of dough made of two different formulae in order to yield distinct consistencies, one being a stiff dough and the other one being a slack dough. Reconstruction and three-dimensional visualization of the internal structure of the dough was accomplished at a resolution of 10 μm^3 per voxel, making possible to resolve gas bubbles as small as 10 μm in diameter. Morphological characterization of the stiff and slack doughs indicated that they entrained bubbles whose size distributions were well defined by a two-parameter lognormal distribution, with geometric mean x_g and geometric standard deviation σ_g. The bubble size distributions in the stiff and slack doughs were found to have similar geometric means, 100 and 109 μm, but quite distinct geometric standard deviation, 1.79 and 1.62, respectively. An analysis of anisotropy of bubble cross-sections (circles 10-μm thick) suggested that the small bubbles entrained in the slack dough were deformed during sample preparation to a greater extent than in the stiff dough, up to a size of 180 μm. Also, the stiff dough entrained a smaller void fraction and fewer bubbles per unit volume than did the slack dough. Furthermore, the distance between adjacent bubbles was obtained, indicating that the bubble separation distribution was normally distributed, with the stiff and slack doughs having a mean separation of 338 and 460 μm and standard deviation of 88 and 156 μm, respectively. Overall, this paper shows how the bubble size distribution in dough can be determined using X-ray microcomputed tomography, opening the possibility to gaining a more comprehensive insight into the aeration phenomenon in wheat flour dough.

Keywords: Dough; Aeration; Bubble size distribution; X-ray microcomputed tomography; Anisotropy

1. Introduction

If breadmaking *can* be characterized as a series of aeration stages (Campbell, Rielly, Fryer, & Sadd, 1998), then the mechanisms by which gas cells in the dough create the cellular structure of the bread crumb need to be studied (Scanlon & Zghal, 2001). Understanding how air bubbles nucleate in the bread dough during mixing is a fundamental first step because it was shown conclusively over 60 years ago that these air bubbles are the only nuclei available for subsequent gas cell growth (Baker & Mize, 1941). A further reason for studying bubbles in dough is that dough exhibits extremely complex rheological properties (Bagley, Dintzis, & Chakrabarti, 1998), and bubble numbers and sizes will affect dough rheology (Bloksma, 1981, 1990; Carlson & Bohlin, 1978). For example, the rate of disproportionation of air bubbles in the dough is influenced by bubble sizes and by the separation between them (van Vliet, 1999), while the number density of bubbles has a remarkable effect on the rheological properties of the dough (Chin, Martin, & Campbell, 2005; Elmehdi, Page, & Scanlon, 2004). Despite the technological and scientific importance of acquiring quantitative data on the bubble size distribution in dough, dough's opacity and fragility have contributed to difficulty in acquiring these data.

* Corresponding author. Tel.: +1 204 474 6480; fax: +1 204 474 7630.
E-mail address: scanlon@cc.umanitoba.ca (M.G. Scanlon).

0963-9969/$ - see front matter © 2006 Published by Elsevier Ltd.
doi:10.1016/j.foodres.2006.07.020

Consequently, very few researchers have investigated bubble size distributions in dough.

In a thorough evaluation of the effect of headspace mixing pressure on gas cell nuclei, Campbell (1991) and Campbell et al. (1991, 1998) used light microscopy to examine sections of frozen dough. They showed that bubble sizes did not change as headspace pressure was varied (Campbell et al., 1998), and that for two types of mixers, mean bubble diameters of 71 and 89 μm were nucleated (Campbell et al., 1991), values close to those of the earliest study reported by Carlson and Bohlin (1978). Subsequent refinement of the pressure mixing studies (Martin, Chin, Campbell, & Morrant, 2004) led to a modification of the conclusion that bubble size was invariant with pressure, since bubble size increased somewhat as mixer headspace pressure increased. Whitworth and Alava (1999) also used light microscopy of frozen sections to show that different mixers altered the void fraction and bubble size cell distributions in doughs prepared with identical ingredients. Optical and stereo microscopy has also been used to examine gas bubble sizes in squashed fresh dough samples made without yeast (Shimiya & Nakamura, 1997). In this case, dough was prepared with a breadmaking machine, and a median bubble diameter of 15 μm was nucleated, but disproportionation increased the median diameter to 35 μm following 100 min of resting of the dough.

Despite the usefulness of these studies for examining how mixing conditions potentially affect crumb cell structure (Campbell, 1991; Carlson & Bohlin, 1978), and for modelling the rheological behaviour of dough (Elmehdi et al., 2004), the validity of these bubble data is questionable since freezing and serial sectioning, or squashing of the dough, invariably affect the integrity of the sample. In addition, reconstruction of bubble size distributions from two-dimensional sections is methodologically difficult (Campbell, Rielly, Fryer, & Sadd, 1999; Martin et al., 2004; Underwood, 1970). Therefore, to unambiguously evaluate the bubble size distributions in the dough, it is desirable if techniques that eliminate additional treatment steps and non-invasively probe the bubble sizes *in situ* are performed.

One technique that has been used to non-invasively interrogate the structure of a number of materials, including cereal-based snack foods (Lim & Barigou, 2004; Trater, Alavi, & Rizvi, 2005) and bread crumb (Falcone et al., 2005), is computerized X-ray microtomography. In this method, a sample is either rotated between a fixed X-ray source and detector or the X-ray source and detector rotate around the specimen. The backprojection data captured at each rotation step is then used to obtain cross-sectional images which can then be used to generate a 3D representation of the scanned object (Cooper, Matyas, Katzenberg, & Hallgrimsson, 2004). A less common technique is to use X-rays from a synchrotron source; monitoring of the expansion of gas bubbles during fermentation has very recently been reported (Babin, Della Valle, Dendievel, Lassoued, & Salvo, 2005), although a description of the initial gas bubble size distribution in the dough was not communicated. In this paper, we report, for the first time, the use of X-ray microtomography to non-invasively evaluate the bubble size distributions in two doughs made from strong breadmaking flour that did not contain yeast. The ingredients for the two doughs were selected in order to create doughs that would be classified as "stiff" and "slack", with a view to understanding how bubble distributions influence the rheology of breadmaking doughs.

2. Materials and methods

A straight grade flour milled from a number 1 grade Canadian Western Red Spring wheat of the 2003 crop year was obtained from the pilot mill of the Canadian International Grains Institute, Winnipeg, MB. Characteristics of the flour are summarized in Table 1.

Doughs were prepared from this flour using one of the following two formulas. Formula A encompassed 100 g flour (14% m.b.), 63.0 g deionised water and 2.40 g NaCl, while Formula B comprised 100 g flour (14% m.b.), 67.4 g deionised water and 0.75 g NaCl. All ingredients were mixed together for 4 min using a GRL 200 mixer (Hlynka & Anderson, 1955) at a constant pin speed of 165 rpm. All dough ingredients were equilibrated overnight to room temperature (22 ± 1 °C) prior to experimentation.

To minimize imaging artefacts arising from relaxation of polymeric constituents in the dough, the doughs were gently placed on a clean plastic surface immediately after mixing and covered with cellophane film (to minimize dehydration) and allowed to rest for approximately 90 min. Four spherical sub-samples were then carefully excised from the experimental doughs using a pair of sharp scissors. Three sub-samples were used for density measurements, which were carried out using a specific gravity method based on

Table 1
Characteristics of the hard red spring wheat flour

Analysis	
Analytical	
Moisture (w.b.), %	14.27
Protein content, %	14.03
Wet Gluten, %	37.8
Dry Gluten, %	13.3
Ash Content, %	0.452
Agtron colour, %	63
Falling number, *s*	428
Minolta colour	
L^*	91.77
a^*	−0.21
b^*	11.20
Farinogram	
Absorption	69.0
Dough development time, min	9.0
Mixing tolerance index (MTI), BU	20
Stability, min	17.9

Archimedes principle of water displacement. The fourth sub-sample was used for the X-ray microtomography scans.

Density measurements based on water displacement were accomplished by excising a dough sub-sample weighing about 2.5 g, which was accurately weighed using a scale precise to ±0.0001 g. The sub-sample was placed in a 25-mL specific gravity bottle previously filled with deionised water, and density calculated from the weight of water displaced. Density was reported as the average of three sub-samples obtained from the same dough batch.

For tomography measurements, a sub-sample (~0.50 g) of the batch of dough was gently squashed between two cellophane layers—aided by two blocks of Plexiglas—to a fixed height (2.17 ± 0.01 mm), and then mounted altogether as a sub-sample-cellophane arrangement into a standard hollow T-shaped sample holder (20.00 mm in diameter) made by SCANCO Medical (Bassersdorf, Switzerland). The cellophane served as an effective moisture loss barrier as well as preventing stickiness-related issues. Squashing was done in every sample prior to its mounting into the sample holder.

Morphological characterization of the dough samples was accomplished at the University of Calgary 3D Morphometrics Laboratory, using the SCANCO Medical VIVACT 40 (Bassersdorf, Switzerland) X-ray microtomograph (μCT) scanner. In this scanner, designed for *in vivo* animal studies, the X-ray source and CCD array detector rotate around a stationary specimen. Reconstruction is *via* a cone-beam algorithm (Kuhn, Goldstein, Feldkamp, Goulet, & Jesion, 1990). Preliminary experiments were carried out to optimize the scanning protocol. Accordingly, we used a peak energy level of 70 kV and a constant current of 109 μA. Analogous characterization techniques to those used in cortical bone analysis, including analogous structural parameters for bone histomorphometry (Parfitt et al., 1987) (Table 2), were implemented to determine the bubble size distribution and void fractions in wheat flour dough.

Sub-samples of the dough were scanned at a spatial resolution of 10 μm. For image acquisition, the scan protocol included rotation through 180° at a rotation step of 0.35°, and an exposure time of 0.205 s per frame. Four-frame averaging was used to improve the signal to noise ratio. Scan times were approximately 420 s. Each μCT scan produced 200 serial cross-sectional 1024 × 1024 pixel images—representing 2 mm along the sample—which collectively resulted in a volume of isotropic 10 μm^3 voxels.

For image processing, the 8-bit grayscale slices were inverted in colour (white to black and *vice versa*) and median filtered (3 × 3 quadratic kernel) to improve the signal to noise ratio using ImageJ 1.35f (http://rsb.info.nih.gov/ij/) (National Institutes of Health, Bethesda, MD, USA). To facilitate 3D morphometric analysis and 3D visualisation of the bubbles, these slices were cropped using a volume of interest (VOI) function, for which the regions of interest (ROI) were interpolated across slices, and then segmented into white and black regions, which represented the bubbles and the dough matrix, using Skyscan® software (CT-Analyser, version 1.4.0.0, Aartselaar, Belgium). The criterion for segmentation of a stack of images was to fix the grayscale threshold value to the minimum value lying in the plateau region that connected the white and black areas of its composite histogram.

For image analysis, the parameters bubble diameter (Bu.Dm), bubble size distribution (Bu.Sd), bubble spacing (Bu.Sp), and bubble number (Bu.N) were measured directly by means of their analogues in trabecular bone analysis (Table 2) using SkyScan software (CT-Analyser, version 1.4.0.0). 3D Renderings of the bubbles were created from the segmented binary images using Skyscan® ANT Visualisation Software (version 2.2.6.0). Anisotropy analysis, where anisotropy was calculated in each slice from the ratio of the major to the minor axis of ellipses fitted to each individual bubble, was carried out using matching rectangular regions of 732 × 120 pixels cropped from the center region of the sample, across 200 serial images, using the particle size function of ImageJ 1.35f. An ellipticity of one denoted a perfectly spherical object.

To construct the frequency distributions, the discrete bubble sizes were tabulated in ascending order of diameter then grouped into size classes (20-μm wide) over the range of bubble sizes observed. The number of observations in each class was then expressed as a percentage of the total and plotted against the midpoint of the class. For the sake of clarity, bubble sizes greater than 320 μm were not plotted but were accounted for in the statistical analysis.

Table 2
Analogous morphological parameters for trabecular bone and bubbles in dough

Trabecular bone	Bubbles in dough
Tissue volume (TV)	Dough volume (DV)
Bone volume (BV)	Bubble volume (BV)
Bone surface (BS)	Bubble surface (BS)
Bone volume fraction (BV/TV)	Bubble volume fraction (BV/DV)
Bone surface to tissue volume (BS/TV)	Bubble surface to dough volume (BS/DV)
Trabecular thickness (Tb.Th)	Bubble diameter (Bu.Dm)
Trabecular separation (Tb.Sp)	Bubble separation (Bu.Sp)

Trabecular bone abbreviations follow standard nomenclature (Parfitt et al., 1987).

3. Results and discussion

3.1. Bubble size distributions

The bubble diameter distribution as seen in the 3D analysis of both doughs is shown in Fig. 1. Bubbles were reconstructed as spheres from the 10-μm thick μCT serial cross-sections (i.e., *slices*) by using a 3D volume reconstruction algorithm (built-in marching cubes algorithm of SkyScan CT-Analyser, version 1.4.0.0). Bubble size distributions were asymmetrical and skewed to the left, suggesting that bubble size distributions were log-normal. Table 3

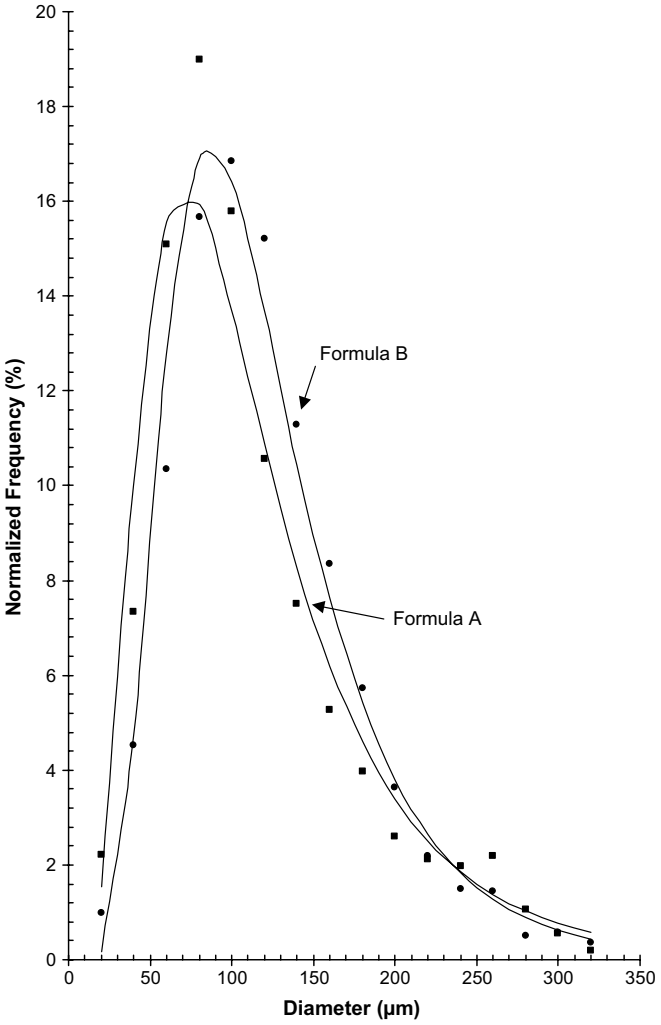

Fig. 1. Bubble size (3D analysis) distribution in doughs prepared with one of two lean bread formulas as determined by X-ray microtomography.

shows the results of the 3D morphometric analyses performed using a combination of μCT scans and powerful software. The scans examined a population of more than 3000 bubbles in each dough.

The two-parameter log-normal distribution used to characterize the bubble distribution was based on equations of Cohen (Cohen, 1988) for the case in which the threshold parameter γ (i.e., the lower limit) was equal to 0. The positive random variable bubble diameter D_i of both doughs was characterized with two parameters, the mean μ and the variance σ^2. This characterization assumes that the random variable, $\ln D_i$, is normally distributed, so that the lines in Fig. 1 are given by the probability density function of D_i and the μ and σ of Table 3

$$f(D_i) = \frac{1}{\sigma \cdot D_i\sqrt{2\pi}} \exp\left(\frac{-(\ln D_i - \mu)^2}{2\sigma^2}\right) \quad (1)$$

where

$f(D_i)$ = probability density function of D_i,
D_i = midpoint of the i-th class in the histogram of bubble sizes,
μ = mean of the log-normal distribution,
σ = standard deviation of the log-normal distribution.

It is worth noting how μ and σ^2 have been derived from the raw data, as this information is not readily available in the literature. For bubble size data grouped into frequency classes the most efficient (maximum likelihood) estimators of μ and σ^2 are as follows:

$$\hat{\mu} = \frac{1}{n}\sum_{i=1}^{k}[\ln D_i * f_i] \quad (2)$$

$$\hat{\sigma}^2 = \frac{1}{n}\sum_{i=1}^{k}[(\ln D_i)^2 * f_i] - \left[\frac{1}{n}\sum_{i=1}^{k}\ln D_i^* f_i\right]^2 \quad (3)$$

Here k is the number of classes, n the size of the sphere population, and f_i the number of spheres falling into class i. Interpretation of data in the log scale, however, is not as transparent and so μ and σ^2 are customarily transformed back into their original scale as follows:

$$x_g = \exp(\mu) \quad (4)$$

$$\sigma_g = \exp(\sigma) \quad (5)$$

Here x_g and σ_g represent the geometric mean and the geometric standard deviation, respectively, of $f(D_i)$.

As with many variables in real life (Crow, 1988; Johannesson & Mitson, 1983; Limpert, Stahel, & Abbt, 2001; Shimizu & Crow, 1988), gas bubble break-up in dough can be viewed as a log-normal phenomenon (Campbell, 1991; Shimiya & Nakamura, 1997). The tomographic analysis on bubble sizes from our experimental slack and stiff doughs (Fig. 1 and Table 3) agrees with this view, suggesting that subdivision of gas bubbles during mixing creates bubbles whose sizes are geometrically proportional. This mechanism operates in keeping with the log normality of the gas bubble size distribution measured, since log

Table 3
Statistical parameters[a] of the best-fit log-normal probability density functions describing experimental bubble size distribution data and void fraction determinations derived from analysis of spheres (3D) by μCT

	Geometric mean (x_g/μm)	Geometric SD (σ_g/μm)	95.5% CL $[x_g/\sigma_g^2 - x_g^*\sigma_g^2]$ (μm)	$\phi_{\mu CT}$ (%)	$\phi_{gravimetric}$ (%)	N (spheres per cm^3)
Formula A	100.0	1.79	31–321	7.64	7.58	30,410
Formula B	109.3	1.62	42–286	9.52	10.41	56,540

[a] $x_g = \exp(\mu)$ and $\sigma_g = \exp(\sigma)$; where μ and σ are respectively the mean and standard deviation of the log-normal distribution fitted to the random variable D_0, the mid-point in the class range (Cohen, 1988; Shimizu & Crow, 1988).

normality has been qualitatively defined by Kolmogoroff (1941) as 'the asymptotic result of an iterative process of successive breakage of a particle into two randomly sized particles' (Shimizu & Crow, 1988).

One important feature of a log normal distribution as compared to a normal distribution is that it has a multiplicative rather than an additive standard deviation. This means, for example, that instead of 95.5% of the random variables being found around a mean ± 2 standard deviations, the same interval of confidence is found for the log normal distribution within the mean multiplied or divided by $(\sigma_g)^2$. This distinction is a key property of the log-normal distribution and leads to the confidence intervals for bubbles in the two doughs shown in Table 3.

The two doughs were made from different formulae in order to produce two distinct consistencies. Based on Bloksma and Bushuk (1988), a water content increase of 1% (flour basis) in a dough formula reduces the stiffness of the dough by 5–15%, so that for these experiments the stiff dough (Formula A) would be about 20–50% stiffer than the slack dough (Formula B). This contrast in consistency was further accentuated by the use of a higher concentration of NaCl in Formula A relative to Formula B, as NaCl stiffens the wheat flour doughs when used at higher concentrations (Bloksma & Bushuk, 1988; Eliasson & Larsson, 1993). It can be observed that using these two different lean formulae to produce a stiff dough and a slack dough, different bubble size distributions were obtained in the doughs (Fig. 1, Table 3). Although the geometric mean has not altered substantially, the stiffer dough's larger geometric SD means that the distribution of bubble sizes is very much broader in the stiffer dough, even though substantially less air was entrained in the dough, as measured by the void fraction (ϕ). The latter result is consistent with dough density measurements of doughs made from flours of different strength (Campbell, Rielly, Fryer, & Sadd, 1993), where stronger (and presumably stiffer) doughs entrained less air.

The void fraction (ϕ) of the doughs was calculated in two ways (Table 3). Firstly, from the ratio (expressed as a percentage) of the total volume of bubble spheres in the scanned dough to that of the total volume of the scanned dough. Secondly, from the density of the dough and its gas-free extrapolation ($\rho_{\text{gas-free dough}}$) determined from gravimetric measurements of the mass and volume of the dough, as follows:

$$\phi_A = 1 - (\rho_A/\rho_{P\text{gas-free dough A}})$$
$$\phi_B = 1 - (\rho_B/\rho_{\text{gas-free dough B}})$$

where $\rho_A = 1190\ \text{kg/m}^3$ (experimentally determined, CV = 2%) and $\rho_{\text{gas-free dough A}} = 1285\ \text{kg/m}^3$ (taken from Elmehdi et al. (2004), as they used the same mixer and formula to prepare their experimental dough). As well, $\rho_B = 1075\ \text{kg/m}^3$, which was experimentally determined (CV=1%), whereas $\rho_{\text{gas-free dough B}}$ was estimated to be $1200\ \text{kg/m}^3$ by using the gas-free density of Formula A dough but accounting for differences in the masses and volumes of NaCl and water between Formulae A and B.

The 3D analysis of the bubbles indicated that the dough made from Formula A (i.e., the stiff dough) had a void fraction of 7.64%, while the gravimetric technique indicated a void fraction of 7.58%. The disparity in void fraction between the two techniques was less than 1%, which translates to an uncertainty of less than 0.1% for the density of the gas-free dough, if it were to be derived from these void fractions. The gas-free dough density of Formula A (the stiff dough), based on a gravimetric-based technique first developed by Campbell (1991), was taken from the work of Elmehdi et al. (2004) using an extrapolation step. The tomography results confirm the validity of this extrapolation.

Although the preparation method for the stiff dough was identical to that of the dough of Elmehdi et al. (2004), their dough had a larger void fraction (8.46%). The smaller amount of gas entrained in our dough may be attributed to a substantial difference in the headspace pressure used during mixing, as our experimental dough was mixed in a city situated at an altitude about 810 m higher than the city in which Elmehdi et al. (2004) mixed their sample—atmospheric pressure drops to $1/e$ of its ground level value at a height of about 8650 m at ambient temperature (Wolfson & Pasachoff, 1987). Accounting for the differences in altitude, and using the empirical relationship between headspace pressure and void fraction determined by Elmehdi et al. (2004), the void fraction of the stiff dough is predicted to drop from 8.46% to 7.70%, a value only slightly greater than what we measured by tomography (7.64%). Other contributing factors also include differences in resting times (i.e., gas losses to the atmosphere) of the dough ex-mixer and variability in the quality of the flour used due to differences in crop years even though both studies used CWRS flour.

For the slack dough, the void fractions measured by μCT compared to those measured by a gravimetric-based technique differed by nearly 9% (Table 3). The 3D analysis determined the density of the gas-free dough to be 1188 kg/m^3 whereas the rule of mixtures estimated it to be 1200 kg/m^3. Here the difference is just under 1%, which does not seem unduly large, but the difference led to an error of about 9% when void fractions were compared. The rule of mixtures should be used with caution as it does not take into account interactions between NaCl and water (e.g., solubility effects) and their interactions with polymers in the dough. For instance, chloride anions have been found to promote the aggregation of gluten proteins (Preston, 1981), suggesting that lowering their concentration in the slack dough (relative to the stiff dough) would result in a dough matrix less dense than that estimated by the rule of mixtures. The matrix (i.e., gas-free dough density) of the slack dough as measured by μCT was indeed less dense than that estimated from the rule of mixtures.

Bubble concentrations, as shown in Table 3, were also determined from these experiments. The stiff dough

entrained nearly half the number of bubbles of that of the slack dough, and had nearly a 20% lower gas content, suggesting that the rheology of breadmaking dough was indeed influenced by the characteristics of the gas phase (and *vice versa*). Martin et al. (2004) observed that aeration of a dough increased when the dough mixer was scaled up, chiefly, due to an increase in the Reynolds number. In the same way, the fewer bubble numbers and lower void fraction of the stiffer dough in the present study may be explained in terms of the Reynolds numbers, as this number decreases when the viscosity (e.g., consistency index) increases.

3.2. Comparison with other research on bubble size distribution in dough

A summary of research where the bubble size distribution in wheat flour doughs was measured is shown in Table 4. Shimiya and Nakamura (1997) found that the bubble size distribution (using circles) in dough changed quickly after mixing due to disproportionation; thus Table 4 includes only their data for 100 min after the end of mixing, which corresponds with the resting time of our doughs (90 min). However, Shimiya and Nakamura (1997) measured bubble (circle) sizes following a simple procedure that likely sacrificed precision, as evidenced by the large disparities between their reported bubble numbers and other previously published data (Table 4). In their technique, a sample was excised immediately after mixing of the dough, squashed between a slide and a cover glass and then directly observed under a microscope or stereoscope (depending on the level of magnification required). The thickness of their slices of dough, however, was fairly large, either 150 or 1000 μm, which in turn limited detection of all bubble circles smaller than the slice thickness, for these circles were not necessarily sectioned and thus analysed. Other bubble size distributions reported in the studies included in Table 4 were obtained by physical sectioning of frozen/unfrozen dough using microtomy. Carlson and Bohlin (1978) found a median bubble size, $\overline{D}$, of 112 μm in dough for which the formula and preparation procedure were not reported. Their one-parameter probability density distribution provided only a location parameter $\overline{D}$ and recognized that the bubble size distribution did not conform to a normal distribution. In addition to a location parameter, a more sophisticated fitting function such as a log-normal density function (Eq. (1)) is also defined by a dispersion parameter (i.e., the standard deviation) which in turn facilitates an adequate characterization of the bubble size population. For instance, the number of bubbles having a particular size could be predicted from these fitting functions using such derived statistics as the intervals of confidence (Table 3).

3.3. Anisotropy analysis

Anisotropy was calculated in each slice from the 3D volumetric data by using the ratio of the major to the minor axis in ellipses fitted to the bubbles. Tomographic slicing occurred in the *xz*-plane of Fig. 2, whereas the dough samples were compressed parallel to the *z*-direction to the fixed height of 2.17 mm. An anisotropy value greater than 1 represented a bubble that had undergone deformation during dough preparation and in which the anisotropy persisted for 90 min after sample preparation (Fig. 2 inset, lower right). The anisotropy analysis indicated that bubble cross-sections were elliptical (Fig. 3). Because anisotropy in small bubbles was prone to large errors due to the inability of pixels (square elements) to adequately follow the contours of a circular geometry, results for bubbles smaller than 80 μm are not included. Fig. 3 shows that bubble cross-sections in the *xz*-plane were more elliptical (more anisotropic) in the slack (Formula B) dough up to bubble sizes of 180 μm, at which point they became essentially similar.

3.4. Bubble separation

Bubble separation is the distance between bubbles within a volume of interest, and is of relevance in calculations of rates of disproportionation of gas bubbles in doughs (van Vliet, 1999). The distributions of distances between bubbles in both doughs were well defined by the normal distribution (Fig. 4). Bubbles were separated by a

Table 4
Literature reports of morphometric analyses of gas bubbles in dough

Reference	Mixer	Maximum resolution (μm)	Slice thickness (μm)	Number of bubbles	ϕ (%)	$\overline{D}$ (μm)	SD (μm)
Carlson and Bohlin (1978)[a]	Not Communicated	90	30	86,700 cm^{-3}	10	112	47.3
Bloksma (1990)	Not communicated	–	–	10^5–10^8 cm^{-3}	10	35	–
Campbell et al. (1991)	Food processor	39	30	78,500 cm^{-3}	2.90	70.9	24.1
Campbell et al. (1991)	Tweedy 10	39	30	33,100 cm^{-3}	2.80	89.4	46.9
Shimiya and Nakamura (1997)[b]	Bread-making machine	3	150	2500 cm^{-2}	3.5	35	1.8[c]

[a] Number of bubbles and mean diameter derived from their proposed probability density function; SD derived using empirical formula proposed by Campbell et al. (1991).

[b] Slice thickness increased to 1 mm when circle diameters >40 μm; ϕ was the total sectional area covered by the circles (m^2/m^2); mean diameter following 100 min resting of dough; $\overline{D}$ was the median diameter in a log-normal distribution (see reference for more details).

[c] It represents a geometric SD (SD = exp (1.8)).

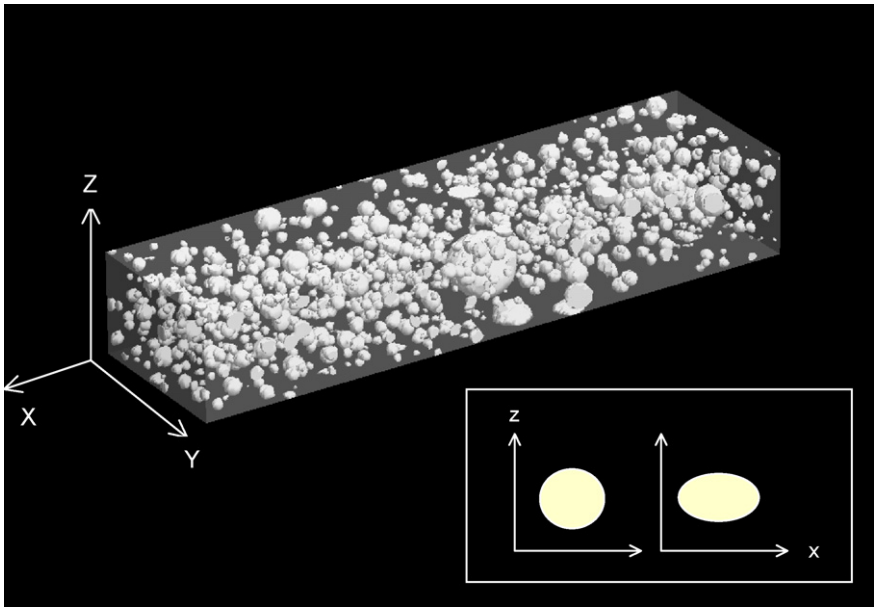

Fig. 2. Spatial rendering of the 3D bubble size distribution in a dough specimen with dimensions (x, y, z) = 732 × 200 × 120 voxels (equivalent to 7.32 × 2.00 × 1.20 mm^3). 200 μCT slices were assembled to produce this rendering using Skyscan® ANT Visualization Software (version 2.2.6.0). Inset at the bottom depicts an isotropic (left) and anisotropic (right) deformation of a bubble as seen in the tomographic slices.

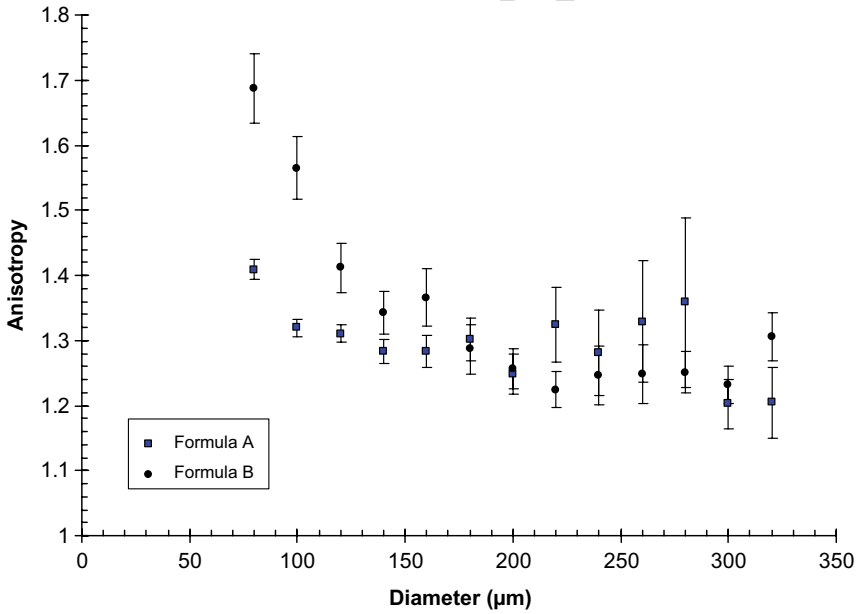

Fig. 3. Anisotropy as a function of bubble sizes in a dough specimen with dimensions 7.32 × 1.20 × 2.00 mm^3. Anisotropy was the ratio of the minor to major axis of best-fitted ellipses to the circle data across 200 serial μCT *slices* (*slice* thickness = 10 μm). Error bars represent 95% confidence limits.

mean distance of 338 μm in the stiff dough (Formula A) and by 460 μm in the slack dough (Formula B) (Table 5). Relative to the mean bubble sizes, the bubble separation analysis suggests that bubbles were discretely separated in both experimental doughs, as the distance between bubbles was on average 3–5 times the size of an average bubble. Bubble separations were more dispersed in the slack dough compared to the stiff dough. This is shown graphically in Fig. 4 and in tabulated form in Table 5.

According to the model of Bloksma (1981) where spherical air bubbles of uniform diameter are arranged cubically (i.e. hexagonal array) in dough, the distance between bubbles (e.g., bubble separation distance) is proportional to both the bubble diameter and a constant $(\pi/\sqrt{18})$ and is inversely proportional to the cubic root of the void fraction. Consequently, Bloskma's model would predict that the stiff and slack doughs had approximately the same separations between bubbles (175 and 177 μm), a prediction

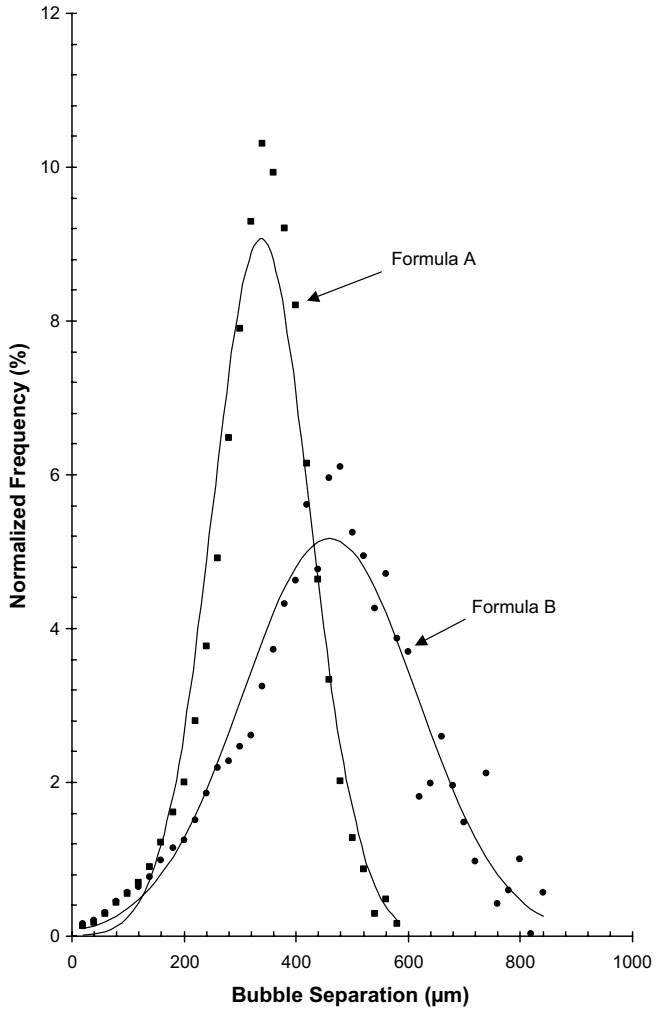

Fig. 4. Bubble separation (3D analysis) distribution in doughs prepared with one of two lean bread formulas. Solid lines represent fits to normal distributions with means μ and standard deviations σ (Table 5).

Table 5
Statistical parameters from the best-fit normal probability density functions used to describe the distribution of separation distances between gas bubbles in dough as detected by 3D analyses on μCT radiographs

	μ (μm)	σ (μm)	95.5% Confidence level (μm)
Formula A	338	88.1	74–602
Formula B	460	155.6	0–936

that is significantly far from the bubble separation distances measured in here by μCT scans (338 and 460 μm). This disparity highlights the importance of integrating information on bubble size distributions in order to develop good mathematical models for predicting the properties of wheat flour dough.

4. Conclusions

These experiments showed how the bubble size distribution in wheat flour dough can be characterized based on information from μCT scans and the use of powerful software. Bubble sizes were reconstructed in three dimensions from circles (i.e., bubble cross-sections) found in 200 μCT slices 10-μm thick of both experimental doughs, without the need to resort to their physical sectioning. The bubble size distribution in the doughs was well described by a two-parameter log-normal density function, with smaller bubble sizes and a wider size distribution in doughs of a stiff consistency. Anisotropy analysis showed that bubbles were deformed in the direction perpendicular to the compressional force (because of sample preparation procedures). Overall results support the view that dough consistency (i.e., viscoelastic properties of the dough) affects the number and size distribution of bubbles that are entrained during mixing. Dough consistency was also found to affect the packing of bubbles as determined by the distribution of distances between bubbles. Bubbles entrained in the stiff dough were dispersed over a narrower range of distances than those in the slack dough. The stiff dough occluded a smaller concentration of bubbles than the slack dough, which is in agreement with reports showing that doughs made from strong breadmaking flours had smaller void fractions than doughs made from weak flours. Establishing a clearer relationship between the degree of dough aeration, the dough formula, and the processing conditions during mixing is a sought-after goal in the baking industry, as it could provide, for example, clues as to how to design more energy efficient dough mixers. The present work suggests that using X-ray microtomography to study bubble size distributions warrants a clearer elucidation of such a relationship.

Acknowledgement

We are grateful for research funding from NSERC's Strategic Grants program and from the Canadian Wheat Board fellowship program.

References

Babin, P., Della Valle, G., Dendievel, R., Lassoued, N., & Salvo, L. (2005). Mechanical properties of bread crumbs from tomography based finite element simulations. *Journal of Materials Science, 40*, 5867–5873.

Bagley, E. B., Dintzis, F. R., & Chakrabarti, S. (1998). Experimental and conceptual problems in the rheological characterization of wheat flour doughs. *Rheologica Acta, 37*, 556–565.

Baker, J. C., & Mize, M. D. (1941). The origin of the gas cell in bread dough. *Cereal Chemistry, 18*, 19–35.

Bloksma, A. H. (1981). Effect of surface tension in the gas-dough interface on the rheological behaviour of dough. *Cereal Chemistry, 58*, 481–486.

Bloksma, A. H. (1990). Dough structure, dough rheology, and baking quality. *Cereal Foods World, 35*, 237–244.

Bloksma, A. H., & Bushuk, W. (1988). Rheology and chemistry of dough (3rd ed.). In Y. Pomeranz (Ed.). *Wheat: chemistry and technology* (Vol. 2, pp. 131–218). St. Paul, MN: American Association of Cereal Chemists, Inc.

Campbell, G.M., (1991). The aeration of bread dough during mixing. Ph.D. Thesis, University of Cambridge.

Campbell, G. M., Rielly, C. D., Fryer, P. J., & Sadd, P. A. (1991). The measurement of bubble size distribution in an opaque food fluid. *Transactions of the Institution of Chemical Engineers, Part C, Food and Bioproducts Processing, 69*, 67–76.

Campbell, G. M., Rielly, C. D., Fryer, P. J., & Sadd, P. A. (1993). Measurement and interpretation of dough densities. *Cereal Chemistry, 70*, 517–521.

Campbell, G. M., Rielly, C. D., Fryer, P. J., & Sadd, P. A. (1998). Aeration of bread dough during mixing: the effect of mixing dough at reduced pressure. *Cereal Foods World, 43*, 163–167.

Campbell, G. M., Rielly, C. D., Fryer, P. J., & Sadd, P. A. (1999). Reconstruction of bubble size distributions from slices. In G. M. Campbell, C. Webb, S. S. Pandiella, & K. Niranjan (Eds.), *Bubbles in food* (pp. 207–220). St. Paul, MN: Eagan Press.

Carlson, T., & Bohlin, L. (1978). Free surface energy in the elasticity of wheat flour dough. *Cereal Chemistry, 55*, 539–544.

Chin, N. L., Martin, P. J., & Campbell, G. M. (2005). Dough aeration and rheology: Part 3. Effect of the presence of gas bubbles in bread dough on measured bulk rheology and work input rate. *Journal of the Science of Food and Agriculture, 85*, 2203–2212.

Cohen, A. C. (1988). Three-parameter estimation. In E. L. Crow & K. Shimizu (Eds.), *Lognormal distributions: theory and applications* (pp. 113–138). New York: Marcel Dekker, Inc.

Cooper, D. M. L., Matyas, J. R., Katzenberg, M. A., & Hallgrimsson, B. (2004). Comparison of microcomputed tomographic and microtomographic measurements of cortical bone porosity. *Calcified Tissue International, 74*, 437–447.

Crow, E. L. (1988). Applications in atmospheric sciences. In E. L. Crow & K. Shimizu (Eds.), *Lognormal distributions: theory and applications* (pp. 331–354). New York: Marcel Dekker, Inc.

Eliasson, A., & Larsson, K. (1993). In *Cereals in breadmaking: a molecular colloidal approach* (pp. 77). New York: Marcel Dekker, Inc.

Elmehdi, H. M., Page, J. H., & Scanlon, M. G. (2004). Ultrasonic investigation of the effect of mixing under reduced pressure on the mechanical properties of bread dough. *Cereal Chemistry, 81*, 504–510.

Falcone, P. M., Baiano, A., Zanini, F., Mancini, L., Tromba, G., Dreossi, D., et al. (2005). Three-dimensional quantitative analysis of bread crumb by X-ray microtomography. *Journal of Food Science, 70*, 265–272.

Hlynka, I., & Anderson, J. A. (1955). Laboratory dough mixer with an air-tight bowl. *Cereal Chemistry, 32*, 83–87.

Johannesson, K. A., & Mitson, R. B., (1983). Fisheries acoustics: a practical manual for aquatic biomass estimation. FAO Fisheries Technical Paper 240. Rome: Food and Agriculture Organization of the United Nations, pp 249.

Kuhn, J. L., Goldstein, S. A., Feldkamp, L. A., Goulet, R. W., & Jesion, G. (1990). Evaluation of a microcomputed tomography system to study trabecular bone structure. *Journal of Orthopaedic Research, 8*, 833–842.

Lim, K. S., & Barigou, M. (2004). X-ray micro-computed tomography of cellular food products. *Food Research International, 37*, 1001–1012.

Limpert, E., Stahel, W. A., & Abbt, M. (2001). Log-normal distributions across the sciences: keys and clues. *BioScience, 51*, 341–352.

Martin, P. J., Chin, N. L., Campbell, G. M., & Morrant, C. J. (2004). Aeration during bread dough mixing. III. Effect of scale-up. *Transactions of the Institution of Chemical Engineers, Part C, Food and Bioproducts Processing, 82*, 282–290.

Parfitt, A. M., Drezner, M. K., Glorieux, F. H., Kanis, J. A., Malluche, H., Meunier, P. J., et al. (1987). Bone morphometry: standardization of nomenclature, symbols and units. *Journal of Bone and Mineral Research, 2*, 595–610.

Preston, K. R. (1981). Effects of neutral salts upon wheat gluten protein properties. I. Relationship between the hydrophobic properties of gluten proteins and their extractability and turbidity in neutral salts. *Cereal Chemistry, 58*, 317–324.

Scanlon, M. G., & Zghal, M. C. (2001). Bread properties and crumb structure. *Food Research International, 34*, 841–864.

Shimiya, Y., & Nakamura, K. (1997). Changes in size of gas cells in dough and bread during breadmaking and calculation of critical size of gas cells that expand. *Journal of Texture Studies, 28*, 273–288.

Shimizu, K., & Crow, E. L. (1988). History, genesis, and properties. In E. L. Crow & K. Shimizu (Eds.), *Lognormal Distributions: Theory and Applications* (pp. 1–26). New York: Marcel Dekker, Inc.

Trater, A. M., Alavi, S., & Rizvi, S. S. H. (2005). Use of non-invasive X-ray microtomography for characterizing microstructure of extruded biopolymer foams. *Food Research International, 38*, 709–719.

Underwood, E. E. (1970). In *Quantitative Stereology* (pp. 274). Reading, MA: Addison-Wesley Publishing Co.

van Vliet, T. (1999). Physical factors determining gas cell stability in a dough during bread making. In G. M. Campbell, C. Webb, S. S. Pandiella, & K. Niranjan (Eds.), *Bubbles in food* (pp. 121–127). St. Paul, MN: Eagan Press.

Whitworth, M. B., & Alava, J. M. (1999). The imaging and measurement of bubbles in bread doughs. In G. M. Campbell, C. Webb, S. S. Pandiella, & K. Niranjan (Eds.), *Bubbles in food* (pp. 221–232). St. Paul, Minnesota: Eagan Press.

Wolfson, R., & Pasachoff, J. M. (1987). In *Physics* (pp. 382). Toronto: Little, Brown, and Company (Canada) Limited.